IJME

*Int. J. of Applied Mechanics and Engineering, 2023, vol.28, No.1, pp.71-83*
DOI: 10.59441/ijame-2023-0007

# SIMILARITY SOLUTION FOR MHD NANOFLUID FLOW WITH HEAT GENERATION IN THE PRESENCE OF RADIATION AND CHEMICAL REACTION EFFECTS

G. PALANI*
Department of Mathematics,
Dr Ambedkar Govt Arts College, Chennai 600039, Tamil Nadu, INDIA.
E-mail: gpalani32@yahoo.co.in

A. ARUTCHELVI
Department of Mathematics,
Bharathi Women's College, Chennai 600108, Tamil Nadu, INDIA.

An analysis has been carried out to study the two-dimensional free convective boundary layer MHD nanofluid flow past an inclined plate with heat generation, chemical reaction and radiation effects under convective boundary conditions. The partial differential equations describing the flow are coupled nonlinear. They have been reduced to nonlinear ordinary differential equations by utilizing a similarity transformation, which is then solved numerically with the aid of the Runge-Kutta-based shooting technique. Graphs depict the influence of different controlling factors on the velocity, temperature, and concentration profiles. Numerical findings for skin friction, Nusselt number and Sherwood number are reviewed for distinct physical parameter values**.** In a limited sense, there is a good correlation between the current study's results and those of the earlier published work**.**

**Key words:** free convection, nanofluid, viscous dissipation, moving inclined plate.

## 1. Introduction

Free convective flows involving simultaneous heat and mass transfer under radiation, chemical reaction, and magnetic fields have been significantly used in numerous engineering and scientific areas. A comprehensive review of the impact of radiation and magnetic fields on a free convective flow has been explored. Many researchers have examined convective boundary conditions in free-convection flows. Aziz [1] came up with the notion of studying a laminar flow across a flat plate with a convective boundary condition. Chamkha [2] investigated a free convective MHD flow in an isothermal inclined surface adjacent to a stratified porous medium. The transfer of heat across a rapidly stretching sheet by the influence of radiation and electromagnetic fields in porosity was investigated by Govind *et al.* [3]. Hari Krishna *et al.* [4] studied the effects of radiation and chemical reactions on the MHD Casson fluid passing through an upright plate in a permeable medium. Kuznetsov and Nield [5] investigated the natural convective boundary-layer flow of a nanofluid past a vertical plate subjected to convective boundary conditions.

Lakshmi *et al.* [6] investigated a numerical solution for MHD flow across a moving upright permeable plate with heat and mass transfer. Mohammed Ibrahim and Bhaskar Reddy [7] focused on how free convective flow across a moving upright plate was influenced by viscous dissipation, chemical reaction, and radiation under convective surface boundary conditions. Makinde [8] examined the MHD heat and mass transmission across a vertical plate. Makinde [9] examined a vertical moving plate with heat generation subject to convective boundary conditions by similarity solution. Manjoolatha *et al.* [10] were interested in the problem of a magnetohydrodynamic flow with heat transfer across a non-isothermal upright plate by the impact of

* To whom correspondence should be addressed

viscous dissipation. Masood Khan *et al.* [11] examined a power-law MHD nanofluid flow with novel mass flux conditions.

Unsteady MHD nanofluid flow of varying characteristics across a stretching sheet with the impact of radiation and the chemical reaction was explored by Musa Antidius Mjankwi *et al.* [12]. Raptis [13] studied the radiation effect on a moving plate of a micropolar fluid. When a magnetic field and radiation are present, heat transport in the unsteady nanofluid was examined by Sheikholeslami and Ganji[14]. An unsteady free convective nanofluid with an MHD effect across a moving upright plate was considered by Sravana Kumar and Rushi Kumar [15]. Srinivas, Reddy, and Prasad [16] examined a magnetohydrodynamic flow across an oblique penetrable stretched surface in the presence of chemical reactions and radiation effects. Srinivas Reddy *et al.* [17] looked into the heat and mass transfer of free convective flow with Dufour and Soret effects past a permeable upright surface. The influence of radiation through a dissipative magneto-nanofluid across a stretching sheet was studied by Syed M. Hussain *et al.* [18]. Vijaykumar and Keshava Reddy [19] analysed the effects of Joule heating and radiation absorption on an MHD flow through an inclined plate. A similarity solution to the unsteady nanofluid flow across an upright plate and convective heating was investigated by Maraka [20].

The current study examines the heat and mass transport of an MHD radiative incompressible nanofluid with convective surface boundary conditions and internal heat generation as it passes through an inclined plate. The implementation of the similarity transformation solves the nonlinear coupled partial differential equations. The shooting technique along with a fourth-order Runge-Kutta scheme is applied to resolve the resultant nonlinear coupled differential equations.

## 2. Mathematical analysis

Consider a free convective flow past an inclined moving plate with a uniform velocity of $U_0$. The flow of the nanofluid is assumed to be a two-dimensional, steady, incompressible, viscous, and electrically conducting . The geometry is set up so that the $x$-axis is measured along the path of the plate and the $y$-axis is orthogonal to it. Here, the plate is expected to be in contact with a cold fluid that is quiescent and has a temperature $T_\infty$ and concentration $C_\infty$. A hot fluid at a temperature $T_f$ heats the plate's left side by convection and produces a heat transmission coefficient of $h_f$, while a cold fluid on the plate's right side produces heat inside at a volumetric rate of $\dot{q}$. The induced magnetic field is ignored and a homogeneous magnetic field $B_0$ is enforced along the $y$-axis. The characteristics of all fluids are believed to be constant.

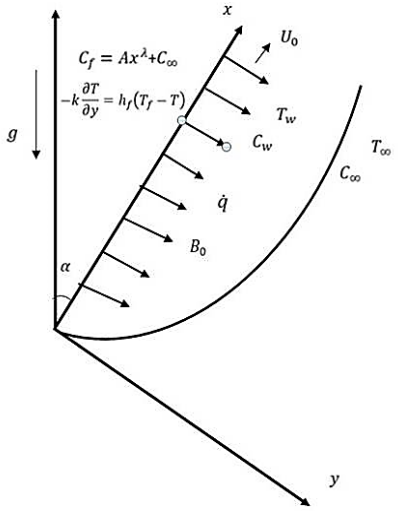


Fig.1. Schematic diagram of the problem.

The nanoparticle considered for this study is copper. Since the base fluid and also the suspended nanoparticles are believed to be in a state of equilibrium, no slip is thought to occur. The flow expressing the equations can be represented using the Boussinesq approximation.

$$\frac{\partial u}{\partial x}+\frac{\partial v}{\partial y}=0, \tag{2.1}$$

$$\begin{aligned}&\rho_{nf}\left(u\frac{\partial u}{\partial x}+v\frac{\partial u}{\partial y}\right)=\\&=\mu_{nf}\frac{\partial^2 u}{\partial y^2}+g\left(\rho\beta_T\right)_{nf}\left(T_f-T_\infty\right)\cos\propto+g\left(\rho\beta_C\right)_{nf}\left(C_w-C_\infty\right)\cos\propto-\sigma_{nf}B_0^2u,\end{aligned} \tag{2.2}$$

$$\left(\rho c_p\right)_{nf}\left(u\frac{\partial T}{\partial x}+v\frac{\partial T}{\partial y}\right)=k_{nf}\frac{\partial^2 T}{\partial y^2}-\frac{\partial q_r}{\partial y}+\dot{q}+\mu_{nf}\left(\frac{\partial u}{\partial y}\right)^2, \tag{2.3}$$

$$\left(u\frac{\partial C}{\partial x}+v\frac{\partial C}{\partial y}\right)=D\frac{\partial^2 C}{\partial y^2}-k_l\left(C_w-C_\infty\right). \tag{2.4}$$

The appropriate boundary conditions are given by,

$$\begin{aligned}&u(x,0)=U_0,\ v(x,0)=0,\ -K_f\frac{\partial T(x,0)}{\partial y}=h_f\left[T_f-T(x,0)\right],\ C_f(x,0)=Ax^\lambda+C_\infty,\\&u(x,\infty)=0,\ T(x,\infty)=T_\infty,\ C(x,\infty)=C_\infty.\end{aligned} \tag{2.5}$$

The following transformations and non-dimensional quantities are introduced,

$$\begin{aligned}&u=U_0f'(\eta),\quad Bi_x=\frac{h_f}{k_f}\left(\frac{x\nu_f}{U_0}\right)^{\frac{1}{2}},\quad v=\frac{\upsilon_f}{2x}\sqrt{\mathrm{Re}_x}\left[\eta f'(\eta)-f(\eta)\right],\quad k_r=\frac{k_l x}{U_0},\\&\eta=y\left(\frac{U_0}{x\nu_f}\right)^{\frac{1}{2}},\quad \theta(\eta)=\frac{T-T_\infty}{T_f-T_\infty},\quad \psi(\eta)=\frac{C-C_\infty}{C_w-C_\infty},\quad Pr=\frac{\nu_f}{\alpha_f},\quad Sc=\frac{\nu_f}{D},\\&Gr_x=\frac{g\left(\beta_T\right)_f\left(T_f-T_\infty\right)x}{U_0^2},\quad Gc_x=\frac{g\left(\beta_C\right)_f\left(C_w-C_\infty\right)x}{U_0^2},\\&Ha_x=\frac{B_0^2\sigma_f x}{\rho_f U_0},\quad S_x=\frac{qx^2e^\eta}{k_f\ \mathrm{Re}_x\left(T_f-T_\infty\right)}.\end{aligned} \tag{2.6}$$

Equation (2.1) is identically satisfied while the Eqs (2.2)-(2.5) are given by:

$$f''' + \frac{1}{2(1-\phi)^{2.5}} \frac{\rho_f}{\rho_{nf}} ff'' + \\ +(1-\phi)^{2.5} \left\{ -\frac{\sigma_{nf}}{\sigma_f} Ha_x f' + \frac{(\rho\beta_T)_{nf}}{(\rho\beta_T)_f} Gr_x \theta \cos\alpha + \frac{(\rho\beta_T)_{nf}}{(\rho\beta_T)_f} Gc_x \psi \cos\alpha \right\} = 0, \tag{2.7}$$

$$\frac{k_{nf}}{k_f} \frac{1}{Pr} \left(1 + \frac{4R}{3}\right) \theta'' = -\left( \frac{(\rho c_p)_{nf}}{(\rho c_p)_f} \frac{f\theta'}{2} + S_x e^{-\eta} + \frac{Ec}{(1-\phi)^{2.5}} (f'')^2 \right), \tag{2.8}$$

$$\psi'' + \frac{1}{2} Scf \psi' - Sck_r \psi = 0, \tag{2.9}$$

$$f(0) = 0, \quad f'(0) = 1, \quad \theta'(0) = -Bi_x \left[1 - \theta(0)\right], \quad \psi(0) = 1, \\ f'(\infty) = 0, \quad \theta(\infty) = 0, \quad \psi(\infty) = 0. \tag{2.10}$$

Equations (2.7) through (2.10) will offer a solution in terms of a local variable, but in order to obtain similarity equations, the factors must be constants rather than functions of $x$. Consequently, we assume:

$$h_f = \frac{a}{\sqrt{x}}, \quad \sigma = \frac{b}{x}, \quad (\beta_T)_f = \frac{c}{x}, \quad (\beta_C)_f = \frac{d}{x}, \quad \dot{q} = \frac{e}{x} e^{-\eta}, \quad k_r = \frac{m}{x}$$

where $a, b, c, d, e$ and $m$ are the constants with appropriate dimensions.
Substituting Eq.(10) into (1), we obtain:

$$Gr = \frac{gc(T_f - T_\infty)}{U_0^2}, \; Gc = \frac{gd(C_w - C_\infty)}{U_0^2}, \; Ha = \frac{bB_0^2}{\rho_f U_0}, \; S = \frac{e\upsilon_f}{k_f U_0 (T_f - T_\infty)}, \; Bi = \frac{a}{k_f} \left( \frac{\nu_f}{U_0} \right)^{\frac{1}{2}}.$$

The following equations are used to determine the Skin friction coefficient, Nusselt number and Sherwood number in terms of respectively in terms of $f''$ and $-\theta'$, respectively:

$$C_f = \frac{f''(0)}{(1-\phi)^{2.5} Re_x^{\frac{1}{2}}}, \quad N_u = -\frac{k_{nf}}{k_f Re_x^{-\frac{1}{2}}} \theta'(0), \qquad Sh_x = -\frac{k_{nf}}{k_f Re_x^{\frac{-1}{2}}} \psi'(0). \tag{2.11}$$

## 3. Solution of the problem

Equations (2.7)-(2.9) constitute nonlinear coupled partial differential equations in conjunction with the boundary constraints (2.10). They are resolved by the shooting technique together with the fourth-order Runge–Kutta integration scheme, which reduces the ordinary differential equations into a set of first-order initial value ordinary differential equations. The values of $f''$, $\theta$ and $\psi$ at $\eta = 0$ are required to solve (2.7) -

(2.9) with (2.10) but they are unknown at the boundaries. So the appropriate assumed values for $f''$, $\theta$ and $\psi$ are selected and then integration is carried out.

## 4. Results and discussion

The impacts of various factors that govern the flow are portrayed in Figs. 2-21. Table 1 compares the findings of the present study to Makinde's work [9]. A good agreement can be seen from the comparison. The numerical values for Skin-friction, Nusselt number and Sherwood number are computed numerically for various values of the parameters $Bi, Gr, Ha, S, R$. These results are presented in Tab.2, and it is noticed that the skin friction decreases with increasing values of $Bi, S, R, \phi$ and $Gr$, however, it rises with an increasing magnetic field. When the $Bi$ and $Gr$ values climb, the Nusselt number rises as well, and simultaneously Nu falls for all other values.

Figures 2 and 3 depict the influence of $Gr$ on the velocity and temperature profiles. The viscosity reduces as buoyant forces grow, which causes the momentum boundary layer to gradually decrease. This will increase the fluid's velocity. The fluid is diluted when its viscosity decreases. The thermal boundary layer thickens, as a result, thereby increasing the temperature.

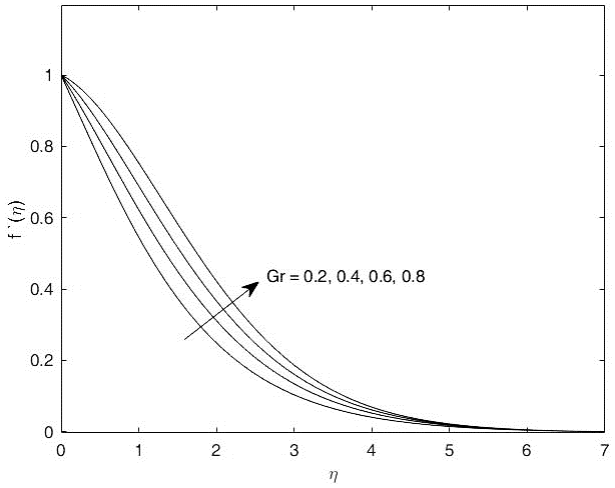


Fig.2. Velocity profile for various values of $Gr$.

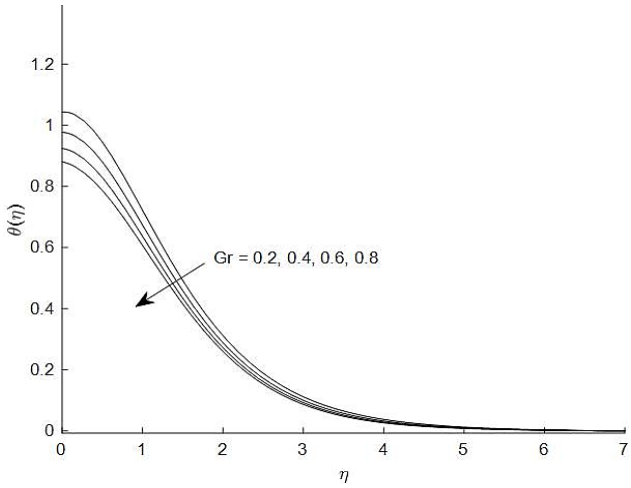


Fig.3.Temperature profile for various values of $Gr$.

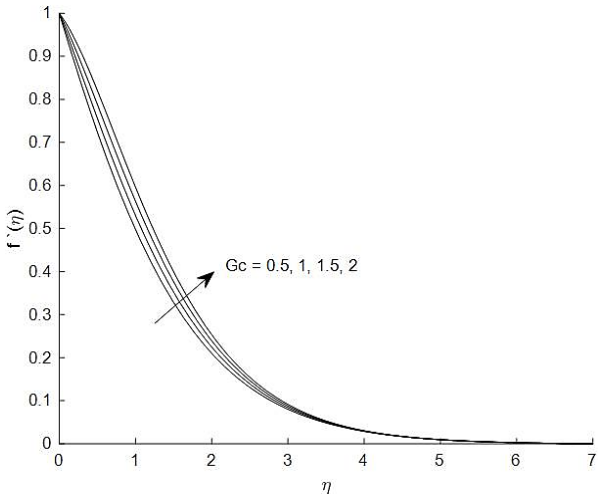


Fig.4. Velocity profile for various values of $Gc$.

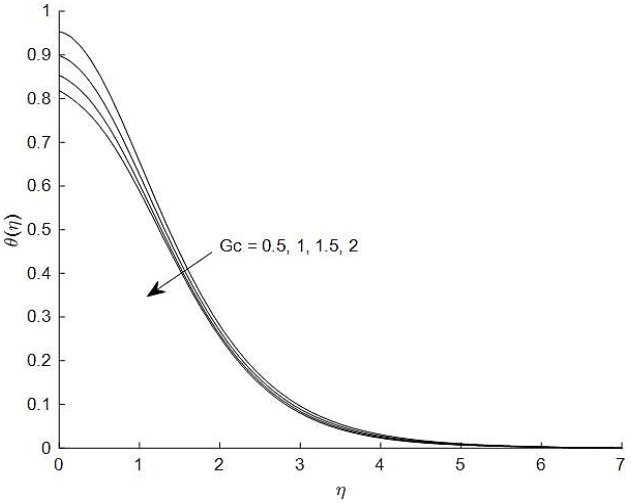


Fig.5. Temperature profile for various values of $Gc$.

Figures 4 and 5 depict how the modified Grashof number affects velocity and temperature fields. It has been noticed that the velocity field rises as $Gc$ rises. It is observed that a rise in $Gc$ causes the temperature to decline.

Figures 6 and 7 depict how the Eckert number affects velocity and temperature. It is observed that when $Ec$ grows, the velocity and temperature profiles of the flow also increase. Here, a positive Eckert number denotes plate cooling, or the transfer of heat to the fluid from a plate. The variations in velocity and temperature fields against the Biot number for the Cu-water nanofluid are shown in Figs 8 and 9. Due to convective energy transport between the hot fluid on the left side of the plate and the cold fluid on the right, the fluid velocity as well as the temperature field drop when the Biot number rises.

Figure 10 shows how magnetic parameters determine the velocity fields when $Ha = 0.2, 0.3, 0.4$ and $0.5$ .This shows that the rise in the magnetic parameters leads to a slowing down of the velocity. The boundary layer's fluid motion tends to be significantly reduced by the Lorenz force, which further increases and tends to enhance the temperature as shown in Fig.11. Figures 12 and 13 demonstrate the impact of $\alpha$ on momentum and temperature respectively. Clearly, the influence of buoyancy force is less when $\alpha$ increases. Furthermore, when the inclination angle grows, the temperature profile also increases, as noticed in Fig.13.

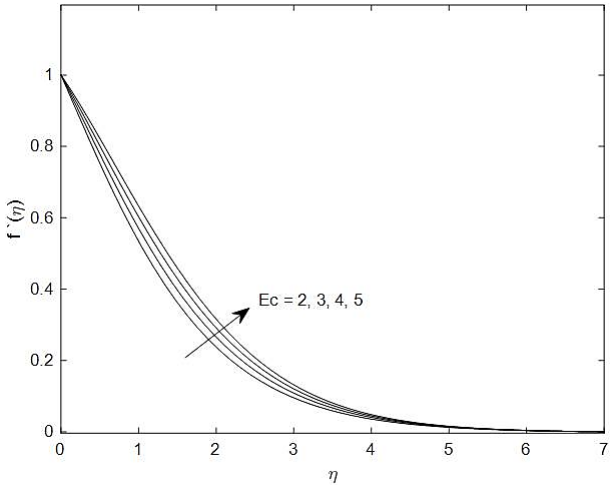


Fig.6. Velocity profile for various values of $Ec$ .

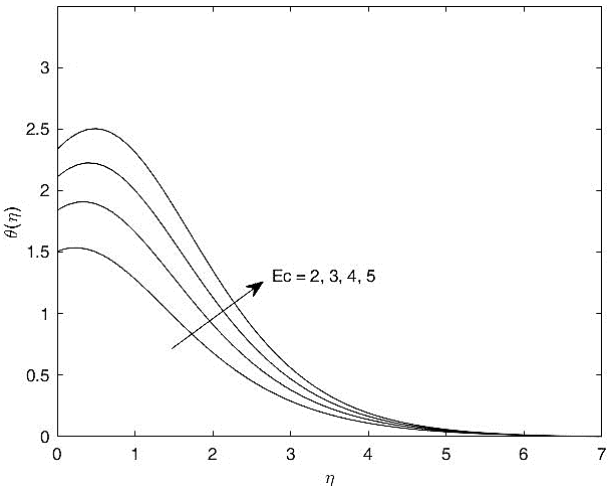


Fig.7. Temperature profile for various values of $Ec$ .

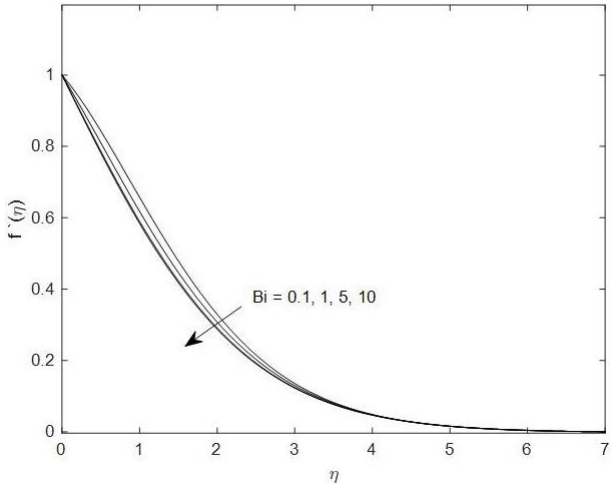


Fig.8. Velocity profile for various of *Bi*.

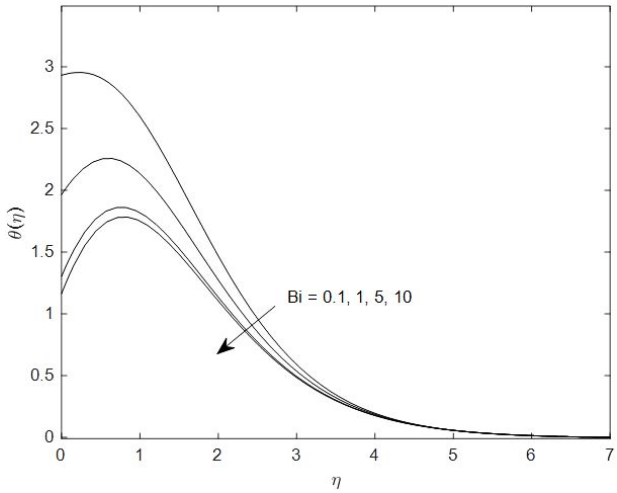


Fig.9.Temperature profile for various values of *Bi*.

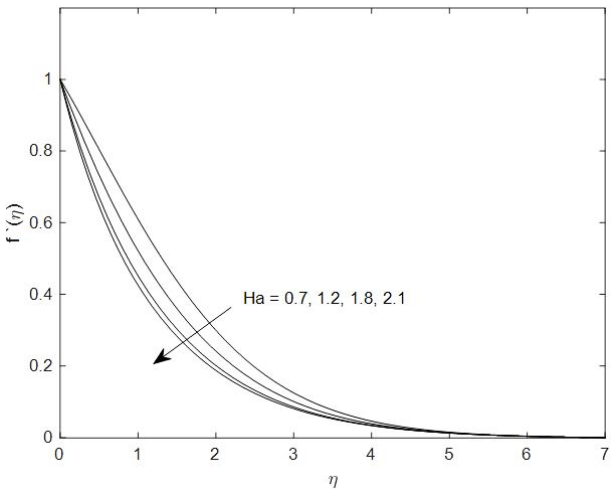


Fig.10. Velocity profile for various values of *Ha*.

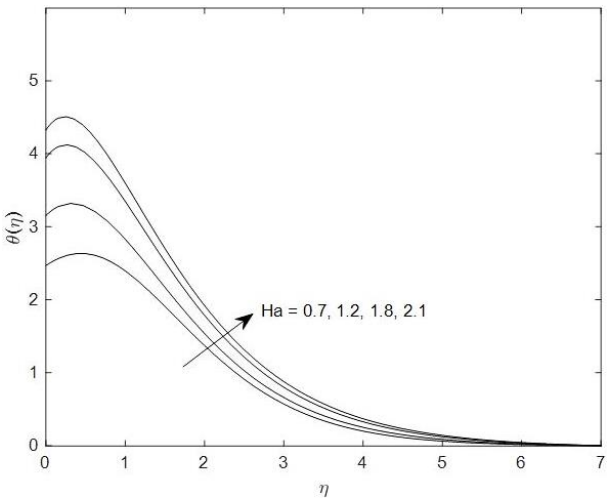


Fig.11. Temperature profile for various values of *Ha*.

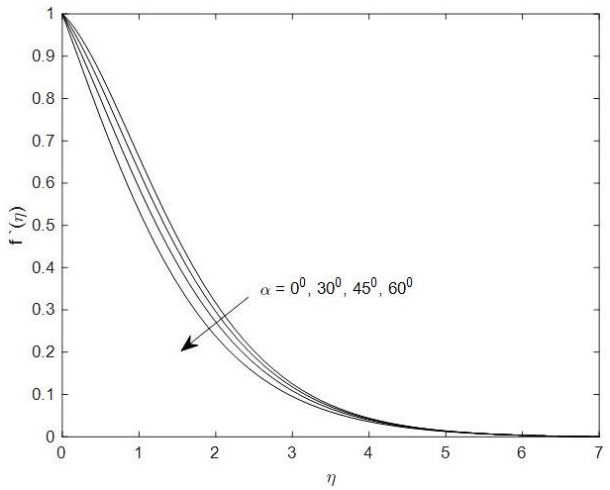


Fig.12. Velocity profile for various values of α.

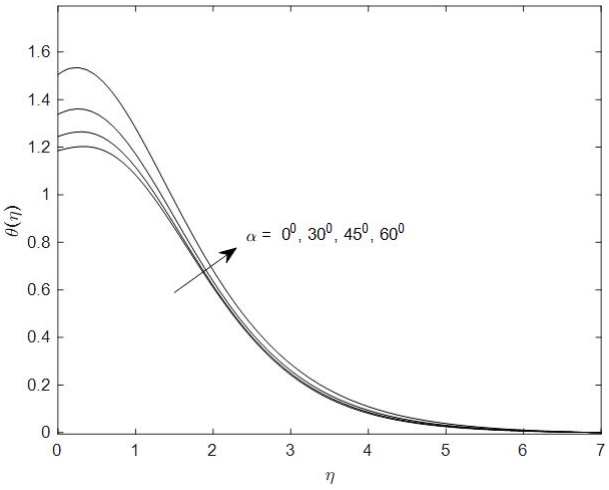


Fig. 13. Temperature profile for various values of α.

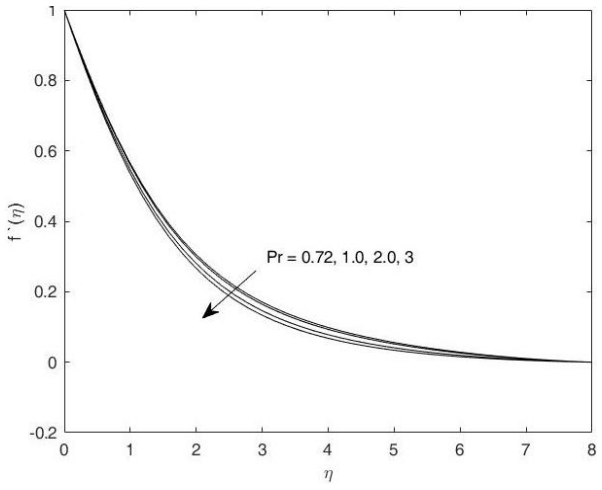


Fig.14. Velocity profile for various values of *Pr*.

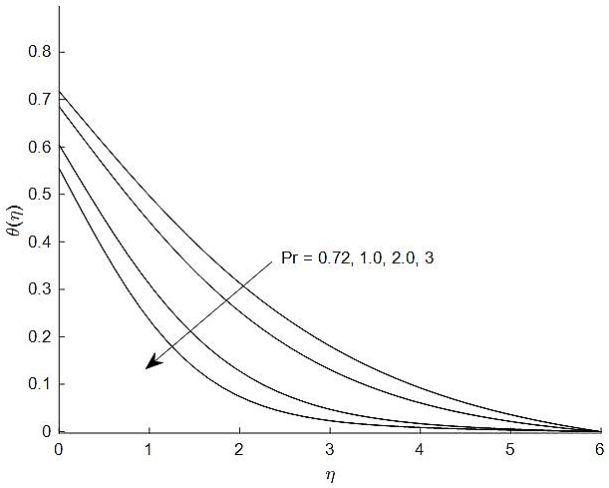


Fig.15. Temperature profile for various values of *Pr*.

Figure 14 brings out the impact of $Pr$ on the fluid velocity field. As $Pr$ increases, the velocity in the boundary layer diminishes. The Prandtl number has a major impact on the temperature profile**.** This is found to be declining as the Prandtl number grows as shown in Fig.15. It causes heat to diffuse more quickly and escape from the heat source more quickly than at higher $Pr$ values. The velocity and temperature fields are depicted in Figs 16 and 17 for different values of the exponentially decaying heat generating factor $S$. The internal heat-generating factor grows while the fluid velocity rises exponentially. The fluid's temperature increases as $S$ rises.

Figure 18 illustrates how the concentration fields are decreasing as the chemical reaction parameters rise. The impact of $Sc$ on the concentration field is shown in Fig.19. The Schmidt number is increasing while the wall concentration field is decreasing. Figures 20 and 21 illustrate how the radiation factor $R$ influences the momentum and temperature profiles for Cu-nanofluids. Raising the radiation parameter has been proven to improve the temperature and velocity fields.

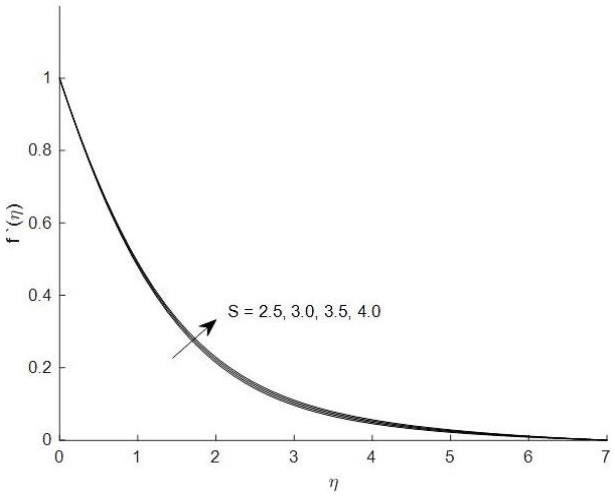


Fig.16. Velocity profile for various values of *S*.

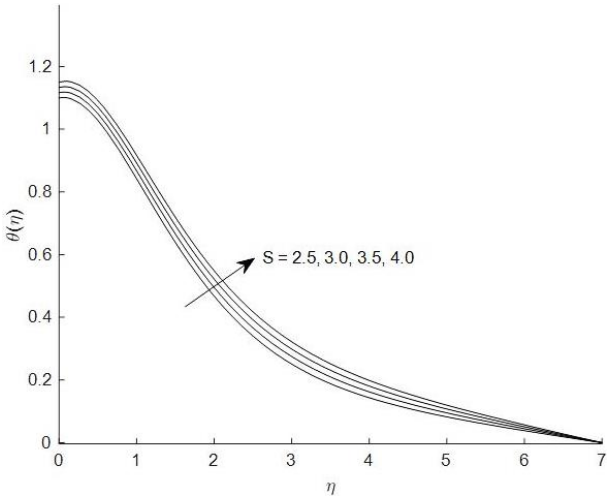


Fig.17. Temperature profile for various values of *S*.

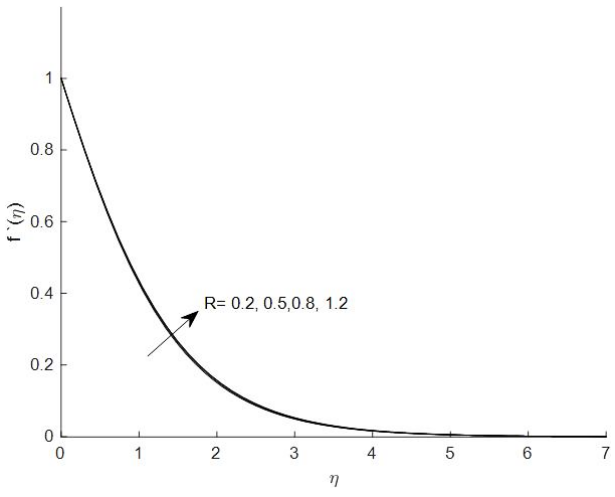


Fig.18. Velocity profile for various values of *R*.

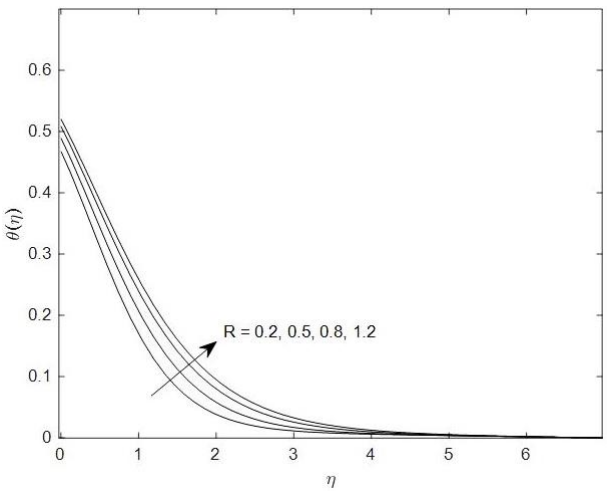


Fig. 19. Temperature profile for various values of *R*.

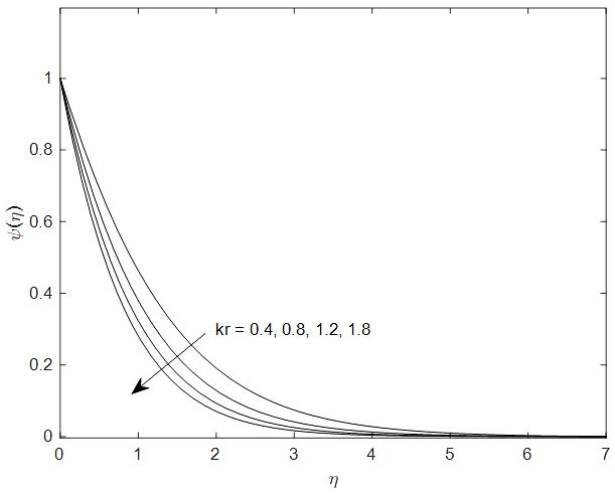


Fig.20. Concentration profile for various values of *kr*.

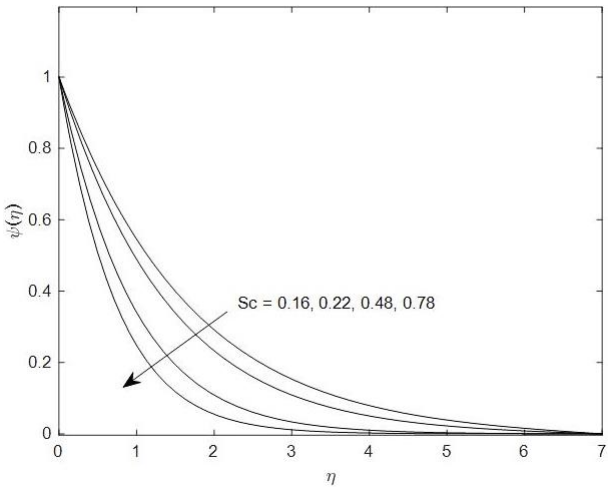


Fig.21. Concentration profile for various values of *Sc*.

Table 1. Comparison value of $f''(0)$ and $\theta'(0)$ for distinct values of $Gr, Pr, Bi, S$ and other values are kept as zero with Makinde [9].

| *Gr* | *Pr* | *Bi* | *S* | $f''(0)$ Makinde [9] | $-\theta'(0)$ Makinde [9] | $f''(0)$ Present work | $-\theta'(0)$ Present work |
|---|---|---|---|---|---|---|---|
| *0.5* | *0.72* | *0.1* | *1* | *0.42212* | *0.04825* | *0.42212* | *0.04825* |
| *1.0* | *0.72* | *0.1* | *1* | *0.98954* | *0.03401* | *0.98954* | *0.03401* |
| *0.1* | *3.0* | *0.1* | *1* | *−0.37486* | *–0.02381* | *−0.37486* | *–0.02381* |
| *0.1* | *7.1* | *0.1* | *1* | *−0.41388* | *–0.05716* | *−0.41388* | *–0.05716* |
| *0.1* | *0.72* | *1.0* | *1* | *−0.24596* | *0.28165* | *−0.24596* | *0.28165* |
| *0.1* | *0.72* | *10* | *1* | *−0.26951* | *0.38295* | *−0.26951* | *0.38295* |
| *0.1* | *0.72* | *0.1* | *5* | *0.37412* | *0.57667* | *0.37412* | *0.57667* |
| *0.1* | *0.72* | *0.1* | *10* | *0.90107* | *1.10660* | *0.90107* | *1.10660* |

Table 2. Computation showing $f''(0), \theta'(0)$ and $\psi'(0)$ and for different physical factors.

| $\phi$ | *Bi* | *Gr* | *Ha* | *S* | *R* | *Sc* | *kr* | $f''(0)$ | $-\theta'(0)$ | $-\psi'(0)$ |
|---|---|---|---|---|---|---|---|---|---|---|
| *0.01* | *0.2* | *0.5* | *0.8* | *1* | *0.1* | *0.78* | *2* | *0.83957* | *0.13985* | *-1.30758* |
| *0.1* | *0.2* | *0.5* | *0.8* | *1* | *0.1* | *0.78* | *2* | *0.82073* | *0.12713* | *-1.30760* |
| *0.2* | *0.2* | *0.5* | *0.8* | *1* | *0.1* | *0.78* | *2* | *0.79835* | *0.11065* | *-1.30788* |
| *0.01* | *1.0* | *0.5* | *0.8* | *1* | *0.1* | *0.78* | *2* | *0.81646* | *0.44770* | *-1.30788* |
| *0.01* | *5.0* | *0.5* | *0.8* | *1* | *0.1* | *0.78* | *2* | *0.79022* | *0.80144* | *-1.30821* |
| *0.01* | *10* | *0.5* | *0.8* | *1* | *0.1* | *0.78* | *2* | *0.78373* | *0.88957* | *-1.30829* |

Cont.Table 2. Computation showing $f''(0), \theta'(0)$ and $\psi'(0)$ and for different physical factors.

| $\phi$ | *Bi* | *Gr* | *Ha* | *S* | *R* | *Sc* | *kr* | $f''(0)$ | $-\theta'(0)$ | $-\psi'(0)$ |
|---|---|---|---|---|---|---|---|---|---|---|
| *0.01* | *0.2* | *1.0* | *0.8* | *1* | *0.1* | *0.78* | *2* | *0.80448* | *0.14129* | *-1.30811* |
| *0.01* | *0.2* | *1.5* | *0.8* | *1* | *0.1* | *0.78* | *2* | *0.77103* | *0.14261* | *-1.30862* |
| *0.01* | *0.2* | *2.0* | *0.8* | *1* | *0.1* | *0.78* | *2* | *0.73902* | *0.14382* | *-1.30910* |
| *0.01* | *0.2* | *0.5* | *2.0* | *1* | *0.1* | *0.78* | *2* | *1.33627* | *0.11333* | *-1.30042* |
| *0.01* | *0.2* | *0.5* | *2.5* | *1* | *0.1* | *0.78* | *2* | *1.49953* | *0.10331* | *-1.29841* |
| *0.01* | *0.2* | *0.5* | *3.0* | *1* | *0.1* | *0.78* | *2* | *1.64781* | *0.93688* | *-1.29671* |
| *0.01* | *0.2* | *0.5* | *0.8* | *2* | *0.1* | *0.78* | *2* | *0.83675* | *0.13768* | *-1.30765* |
| *0.01* | *0.2* | *0.5* | *0.8* | *3* | *0.1* | *0.78* | *2* | *0.83397* | *0.13553* | *-1.30771* |
| *0.01* | *0.2* | *0.5* | *0.8* | *4* | *0.1* | *0.78* | *2* | *0.83120* | *0.13340* | *-1.30777* |
| *0.01* | *0.2* | *0.5* | *0.8* | *1* | *0.5* | *0.78* | *2* | *0.83484* | *0.13766* | *-1.30773* |
| *0.01* | *0.2* | *0.5* | *0.8* | *1* | *1.0* | *0.78* | *2* | *0.82924* | *0.13458* | *-1.30787* |
| *0.01* | *0.2* | *0.5* | *0.8* | *1* | *2.0* | *0.78* | *2* | *0.81905* | *0.12856* | *-1.30810* |
| *0.01* | *0.2* | *0.5* | *0.8* | *1* | *0.1* | *0.22* | *2* | *0.79348* | *0.14371* | *-0.68920* |
| *0.01* | *0.2* | *0.5* | *0.8* | *1* | *0.1* | *0.60* | *2* | *0.83027* | *0.14057* | *-1.14510* |
| *0.01* | *0.2* | *0.5* | *0.8* | *1* | *0.1* | *2.0* | *2* | *0.87024* | *0.13773* | *-2.10384* |
| *0.01* | *0.2* | *0.5* | *0.8* | *1* | *0.1* | *0.78* | *3* | *1.51521* | *0.88400* | *-2.52673* |
| *0.01* | *0.2* | *0.5* | *0.8* | *1* | *0.1* | *0.78* | *4* | *1.52828* | *0.90498* | *-2.89763* |
| *0.01* | *0.2* | *0.5* | *0.8* | *1* | *0.1* | *0.78* | *5* | *1.76202* | *2.42747* | *-3.226036* |

## 4. Conclusion

The steady laminar incompressible MHD nanofluid flow past an inclined moving plate with internal heat generation, viscous dissipation, chemical reaction, and radiation effects under convective boundary conditions has been investigated numerically. The shooting technique and the fourth-order Runge-Kutta integration scheme are used to solve nonlinear coupled governing partial differential equations. The important findings of the investigation from graphical representations are listed below.

1. Velocity increases when $Gr, Gc$ and $S$ increase.
2. Velocity decreases when $M, Pr, Sc$ and $kr$ increase.
3. Temperature increases as $M, S, Sc$ and $kr$ increase.
4. Temperature decreases as $Gr, Gc$ and $Pr$ increase.
5. Concentration decreases when $M, S, Sc$ and $kr$ increase.

## Acknowledgements

We would like to extend our sincere appreciation to the reviewers for their thoughtful comments and efforts toward improving our manuscript. Also, we would like to express our gratitude to the Department of Mathematics, Dr. Ambedkar Govt Arts College, Chennai 600039, Tamil Nadu, INDIA and the Department of Mathematics, Bharathi Women's College, Chennai 600108, Tamil Nadu, INDIA for their continuous support.

## Nomenclature

$Bi$ – Biot number
$B_0$ – magnetic induction
$C_w$ – concentration of the fluid near the plate
$C_\infty$ – free stream concentration
$(c_p)_{nf}$ – specific heat capacity of the nanofluid
$D$ – mass diffusivity
$kr$ – chemical reaction parameter
$k_f$ – thermal conductivity of the base fluid
$k_{nf}$ – thermal conductivity of the nanofluid
$Gr$ – buoyancy ratio parameter
$Nu_x$ – local Nusselt number [
Pr – Prandtl number
$q$ – heat generation term
$R$ – radiation parameter
$Sc$ – Schmidt number
$T_f$ – temperature of the hot fluid
$T_w$ – temperature of the fluid near the plate
$T_\infty$ – temperature of the fluid away from the plate
$u$ , $v$ – the velocity components in the coordinate system
$\alpha$ – inclination parameter
$(\beta_C)_{nf}$ – solute expansion coefficient
$(\beta_T)_{nf}$ – thermal expansions coefficients
$\lambda$ – the plate surface concentration exponent
$\mu_f$ – viscosity of the base fluid
$\mu_{nf}$ – dynamic viscosity of the nanofluid
$\rho_f$ – density of the base fluid
$\rho_{nf}$ – density of the nanofluid
$(\rho c_p)_{nf}$ – heat capacitance of nanofluid
$\sigma^*$ – Stefan- Boltzmann constant

$\sigma_{nf}$ – electrical conductivity of the nanofluid

$\tau_x$ – local skin friction coefficient

$\upsilon_f$ – kinematic viscosity of the base fluid

$\varphi$ – solid volume fraction

## References

[1] Aziz A. (2009): *A similarity solution for laminar thermal boundary layer over a flat plate with a convective surface boundary condition*.– Comm. Nonlinear Sci. and Num. Siml., vol.14, No.4, pp.1064-1068.

[2] Chamkha A.J. (1997): *Hydromagnetic natural convection from an isothermal inclined surface adjacent to a thermally stratified porous medium*.– Int. J. Engng Sci., vol.35, pp.975-986.

[3] Rajput G.R., Jadhav B.P. and Salunkhe S.N. (2020): *Magnetohydrodynamics boundary layer flow and heat transfer in porous medium past an exponentially stretching sheet under the influence of radiation.*– Heat Transfer,vol.49, No.5, pp.2906-2920.

[4] Krishna Y.H., Bindu P., Vijaya N. and Reddy G.R. (2019): *Radiation and chemical reaction effects on the boundary layer MHD Casson fluid on a vertical plate embedded in the porous medium*.– Int. J. Mech. Engng. Technol., vol.10, pp.1-12.

[5] Kuznetsov A.V. and Nield D. A. (2010): *Natural convective boundary-layer flow of a nanofluid past a vertical plate.*– Int. J. Thermal Sci., vol.49, No.2, pp.243-247.

[6] Lakshmi R., Jayarami K.R., Ramakrishna K. and Reddy G.R. (2014): *Numerical Solution of MHD flow over a moving vertical porous plate with heat and Mass Transfer*.– Int.J.Chem.Sci.,vol.12, No.14, pp.1487- 1499.

[7] Ibrahim S.M. and Reddy B.N. (2013): *Similarity solution of heat and mass transfer for natural convection over a moving vertical plate with internal heat generation and a convective boundary condition in the presence of thermal radiation, viscous dissipation, and chemical reaction*.– Int. Scholarly Research Notices., doi.org/10.1155/2013/790604.

[8] Makinde O.D. (2010): *On MHD heat and mass transfer over a moving vertical plate with a convective surface boundary condition*.– The Canadian J. Chem. Engng., vol.88, No.6, pp.983-990.

[9] Makinde O.D. (2011): *Similarity solution for natural convection from a moving vertical plate with internal heat generation and a convective boundary condition*.– Thermal Science., vol.15, pp.137-143.

[10] Manjoolatha E., Suneetha S., Prasanna Lakshmi M. and Bhaskar Reddy N. (2015): *Soret and Dufour effects on MHD heat and mass transfer flow over a moving non-isothermal vertical plate with thermal stratification and viscous dissipation*.– Int. J. Innovative Sci. Engng. & Tech., vol.2, No.8, pp.866-879.

[11] Khan M. and Khan W.A. (2016): *MHD boundary layer flow of a power-law nanofluid with new mass flux condition.*– AIP Advances, vol.6, No.2, p.025211.

[12] Mjankwi M.A., Masanja V.G., Mureithi E.W. and James M.N.O. (2019): *Unsteady MHD flow of nanofluid with variable properties over a stretching sheet in the presence of thermal radiation and chemical reaction*.– Int. J. Mathematics and Mathematical Sci., doi.org/10.1155/2019/7392459.

[13] Raptis A. (1998): *A flow of a micropolar fluid past a continuously moving plate by the presence of radiation.*– Int. J. Heat and Mass Transfer., vol.41, No.18, pp.2865-2866.

[14] Sheikholeslami M. and Ganji D.D. (2015): *Unsteady nanofluid flow and heat transfer in presence of magnetic field considering thermal radiation.*– J. Brazilian Soc. Mech. Sci. and Engng., vol.37, No.3, pp.895-902.

[15] Sravan Kumar T. and Rushi Kumar B. (2017): *Unsteady MHD free convective boundary layer flow of a nanofluid past a moving vertical plate.*– IOP Conf. Series: Materials Science and Eng., doi:10.1088/1757-899X/263/6/062015

[16] Srinivas S., Reddy P.B.A. and Prasad B.S.R.V. (2014): *Effects of chemical reaction and thermal radiation on MHD flow over an inclined permeable stretching surface with non-uniform heat source/sink: An application to the dynamics of blood flow.*– J. Mech. Medicine and Biology., vol.14, No.5, p.1450067.

[17] Reddy D. S. and Govardhan K. (2015): *Effect of viscous dissipation, Soret and Dufour effect on free convection heat and mass transfer from vertical surface in a porous medium*.– Procedia Materials Sci. vol.10, pp. 563-571.

[18] Hussain S.M., Sharma R., Seth G.S. and Mishra M.R. (2018): *Thermal radiation impact on boundary layer dissipative flow of magneto-nanofluid over an exponentially stretching sheet*.– Int. J. Heat Tech., vol.36, No.4, pp.1163-1173.

[19] Vijaykumar K. and Keshava Reddy E. (2017): *Joule heating and radiation absorption effects on MHD convective and chemically reactive flow past an inclined porous plate*.– Int. J. Research and Scientific Innovation., vol.4, No.8, pp.66-74.

[20] Maraka W.M., Ngugi K.M. and Roy K.P. (2018): *Similarity solution of unsteady boundary layer flow of nanofluids past a vertical plate with convective heating*.– Global J. Pure and App. Math., vol.14, No.4, pp.517-534.

Received: September 9, 2022
Revised: January 19, 2023